scientific reports

Check for updates

OPEN

Nilotinib hydrochloride monohydrate solubility in supercritical carbon dioxide + cosolvent: measurements and modeling

Seyed Ali Sajadian[1]✉, Adel Noubigh[2], Mahshid Askarizadeh[3] & L. Antonio Estévez[4]✉

The solubility of nilotinib hydrochloride monohydrate in supercritical CO_2 was measured at four temperatures between 338 K and 308 K, and seven pressures between 12 MPa and 30 MPa, using ethanol as a cosolvent. Both semi-empirical and empirical approaches were employed to analyze the experimental data. In the ternary systems studied, the solubility values (mole basis) for nilotinib hydrochloride monohydrate were between 1.08×10^{-5} and 4.15×10^{-4} (10.8 to 415 PPM). The results indicated a significant increase in solubility with the incorporation of ethanol. The peak solubility of nilotinib hydrochloride monohydrate was recorded in the ternary system at 338 K and 12 MPa, which was approximately 10.8 times its solubility in supercritical carbon dioxide alone under identical conditions. The best fit for the data, as measured by the average absolute relative deviation percentage (*AARD*%), was achieved using the methods proposed by MST.

Keywords Nilotinib hydrochloride monohydrate, Solubility measurement, Supercritical carbon dioxide, Cosolvent, Semi-empirical modeling

Nilotinib hydrochloride monohydrate, (NHM), sometimes called nilotinib monohydrochloride monohydrate, exhibits a bioavailability of approximately 25% or lower and is classified as category IV in the biopharmaceutics classification system (BCS) due to its low solubility and intestinal permeability, indicating that its absorption is limited by solubility. Nilotinib is a yellow powdered pharmaceutical compound, classified as monohydrate monohydrochloride; its solubility in water diminishes as the pH level rises. The chemical designation is 4-methyl-N-[3-(4-methyl-1 H-imidazol-1-yl)-5-(trifluoromethyl) phenyl]-3-[4-(3-pyridinyl)-2-pyrimidinyl] amino]-benzamide, monohydrochloride, monohydrate. It is asserted that crystalline form B of nilotinib hydrochloride monohydrate exhibits enhanced crystallinity and greater physical stability compared to other polymorphic forms. The research by Herbrink et al.[1] was aimed at improving NHM's solubility and absorption through a new spray-dried solid-dispersion method. They created solid dispersions of NHM using effective polymers and evaluated the formulations' dissolution and physicochemical properties using various techniques. Their results showed that a spray-dried, solid-dispersion formulation of NHM with Soluplus® in a 1:7 ratio significantly enhanced its dissolvability. Nilotinib is a multi-targeted protein kinase inhibitor that is structurally related to imatinib mesylate and dasatinib[2–7].

Supercritical fluid (SCF) technology, particularly when using supercritical carbon dioxide ($scCO_2$), is highly flexible and beneficial for pharmaceutical applications. $ScCO_2$ has unique properties, combining aspects of gases and liquids, and is favored for its safety, non-flammability, nontoxicity, and cost-effectiveness. It is beneficial for producing heat-sensitive medications, such as peptides and proteins, and can be easily and completely removed from the system without leaving traces of it[8–17]. A strategy using SCF can improve the solubility and pharmacokinetics of lipophilic drugs, especially those in BCS classes II and IV. The solubility of these drugs in SCF is crucial for pharmaceutical development.

[1]Department of Chemical Engineering, Faculty of Engineering, University of Kashan, Kashan 87317-53153, Iran. [2]Center for Scientific Research and Entrepreneurship, Northern Border University, Arar 73213, Saudi Arabia. [3]Department of Chemical Engineering, Marv.C., Islamic Azad University, Marvdasht, Iran. [4]Department of Chemical Engineering, University of Puerto Rico, Mayagüez 00681-9000, Puerto Rico. ✉email: seyedali.sajadian@gmail.com; antonio.estevez@upr.edu

Solubility experiments can be performed statically or dynamically, employing quantifying methods such as gravimetric, spectrometric, and chromatographic techniques[12,14,18–28]. Precise solubility data are crucial to effectively leverage supercritical technology in drug treatment, as it dictates the drug's affinity with the chosen solvent and therefore helps in its selection.

There are three primary methods for particle production: (i) employing SCF as a solvent through techniques such as rapid expansion of supercritical solution (RESS), (ii) utilizing SCF as an anti-solvent with methods like gas antisolvent (GAS) and supercritical antisolvent (SAS), and (iii) using SCF as a cosolvent with strategies like particles from the gas saturated solution (PGSS). A thorough understanding of these processes requires the extent to which a solute is dissolved in the SCF. Therefore, it is essential for researchers and professionals in the field[10,12,29–39].

Pharmaceutical researchers utilize modeling techniques to assess drug solubility, thereby minimizing both time and costs. They employ cubic equations of state (cEoS) and solution models that incorporate fugacity and activity coefficients to analyze thermodynamic behaviors. While cEoS involves intricate mixing rules and estimated variables, solution models focus on readily measurable properties such as melting point and fusion enthalpy. There is an opportunity to improve empirical and semi-empirical models, which depend on independent variables like the density of pure $scCO_2$, temperature, and pressure, rather than requiring in-depth knowledge of the characteristics of solid solute drugs[40–42].

The solubility of a medicinal compound in $scCO_2$ is crucial for choosing nanoparticle production methods[43–47]. Sajadian et al.[5]. measured NHM solubility in $scCO_2$ (binary system: NHM-$scCO_2$) with mole fraction ranging from 1×10^{-6} to 7.36×10^{-5}.

Numerous studies highlight a key challenge in SCF processes: the limited ability of $scCO_2$ to dissolve hydrophilic and polar solutes. Despite many medications being polar molecules, their nonpolar nature makes it difficult to dissolve in carbon dioxide. To address this issue, $scCO_2$ is often combined with cosolvents, which improves solubility for both polar and non-polar substances. Research indicates that adding small amounts (less than 10%) of polar solvents such as menthol, acetone, methanol, DMSO, and ethanol, can significantly enhance the dissolution of solutes in $scCO_2$[43–49]. Cosolvent addition can enhance process efficiency by improving selectivity and increasing solvent loading, but it may complicate product recovery and process design. Evaluating its benefits requires careful consideration of its pros and cons, as well as a thorough understanding of its impact on solubility, mass transfer, and costs. Cosolvents can improve the solvation power of less soluble compounds in supercritical fluids through intermolecular interactions and hydrogen bonding, while increased solvent density and specific interactions with components can enhance separation selectivity, making cosolvents useful in various applications[43,47,50–52].

Cosolvents significantly impact intermolecular interactions and density, improving solubility and selectivity in ternary systems (ternary system: NHM-$scCO_2$-cosolvent). Small amounts of cosolvent can greatly enhance the solvent power of $scCO_2$. However, their effectiveness depends on the concentration in the supercritical phase, and the mixtures must be supercritical and fully miscible to achieve optimal results[51–56]. The cosolvent effect is primarily influenced by solvent density and enhanced intermolecular interactions. While multicomponent systems can achieve greater solubility, increased density of the solvent mixture does not improve selectivity. Factors like pressure and temperature impact how a cosolvent affects solvent density. When a cosolvent is added, it becomes denser, causing surrounding SCF molecules to cluster, which increases the SCF bulk density. The most significant density increase occurs near the critical point of the solvent mixture. As pressure increases, density of the SCF and its mixture eventually converge, leading to reduced clustering and a rise in SCF density, which decreases the density difference between the cosolvent and the SCF[51–58].

Hydrogen bonding (H-bonding) is an interaction between hydrogen bond donors (HBD) and acceptors. It occurs when a highly electronegative atom in a covalent bond attracts electrons, partially exposing the proton. The acceptor must have polarizable or lone-pair electrons to interact with the donor. Functional groups like alcohols, water (OH), and carboxylic acids can act as both donors and acceptors, while some, like the C=O in carboxylic acids, serve only as acceptors. Common H-bonds are moderate interactions between neutral donors and acceptor groups, such as O=C and OH, which are prevalent in nature and science[53]. Studies show that hydrogen bonding between a solute and a supercritical fluid occurs even at low pressures and remains largely stable despite pressure changes. This aligns with the law of mass action. As the solvent concentration is much higher than that of the solute, a minimal equilibrium shift is observed with increasingly solvent concentration. To investigate the impact of solvents on hydrogen bonding and clustering, specific criteria were established: (i) solutes must be soluble in liquid, supercritical, and gas phases; (ii) solutes should have minimal self-association; (iii) solvents should lack HBD or acceptor (HBA) properties; (iv) solvents must be transparent in relevant spectral regions; and (v) the critical point of the solvent mixture should be close to that of the solvent itself to ensure significant compressibility[59].

Ethanol is commonly used as a cosolvent when dealing with pharmaceuticals due to its low health risks. In 2023, Manna and Banchero[60] studied the solubility of hydrocortisone and cortisone in $scCO_2$ with ethanol as a cosolvent. They found that both Garlapati-Madras[51] and Reddy-Madras[61] models best correlated the ternary system for both compounds, emphasizing the significance of safe and effective cosolvents in pharmaceutical applications[60]. A recent study[51] found that ethanol is an effective cosolvent for nystatin, increasing its solubility in $scCO_2$ by at least 8.7 times. The best models for correlating the ternary system were developed by Jouyban et al.[62]. and Garlapati-Madras[63]. Sajadian et al.[64] explores the solubility of mesalazine in $scCO_2$ with and without a cosolvent, examining temperatures from 308 to 338 K and pressures from 12 to 30 MPa. The solubility of mesalazine in $scCO_2$ was found to range from 4.41×10^{-5} to 18.4×10^{-5} mole fractions, (44.1 to 184 ppm), depending on temperature. The addition of 2% dimethyl sulfoxide as a cosolvent significantly enhanced solubility, increasing the range to between 28.2×10^{-5} and 82.6×10^{-5}. A novel association model was used to correlate the solubility data for both binary and ternary systems, alongside various several semiempirical

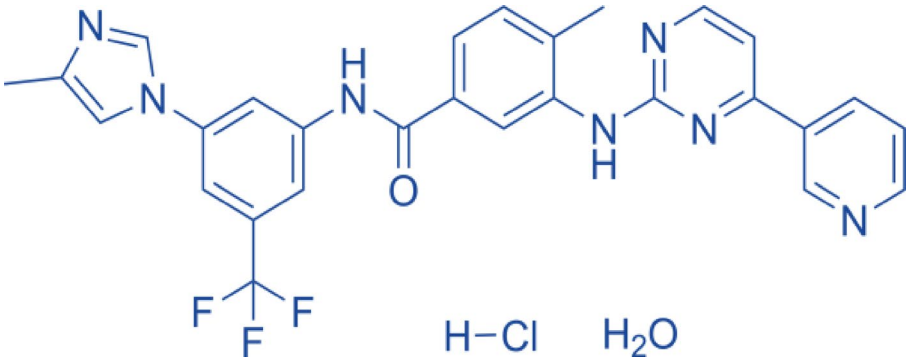

Fig. 1. Structure of nilotinib hydrochloride monohydrate.

Material	Source	Purity (mass basis)	Analysis method
Nilotinib hydrochloride monohydrate	Tofigh Daru Research & Engineering Co.	< 0.991	HPLC
Ethanol	Merck Co.	0.999	GC
Carbon dioxide	Shiraz Aboughaddareh Industrial Gas Co.	0.999	GC

Table 1. Sources and purity of the materials used in this work.

correlations for solubility calculations[64]. Research indicates that incorporating ethanol as a cosolvent enhances the solubility of alprazolam and rivaroxaban in $scCO_2$ by 16.63 and 18.73 times, respectively. The Soltani and Mazloumi[65], Garlapati-Madras[63], and Sodeifian-Sajadian[66] models are the most accurate for rivaroxaban, while the Garlapati-Madras[63] model is the best for alprazolam[67,68]. The solubility of teriflunomide in $scCO_2$ was examined at temperatures of 338, 328, 318, and 308 K, both with and without ethanol as a cosolvent. The presence of ethanol significantly enhanced teriflunomide's solubility, peaking at 338 K and 12 MPa, where it was approximately 14 times higher than in pure $scCO_2$[69].

Ethanol has been frequently used as a cosolvent, and this study is aimed at deepening our understanding of NHM solubility in $scCO_2$. Static equilibrium tests were conducted at seven pressures ranging from 12 to 30 MPa and four temperatures (308, 318, 328, and 338 K). The investigation focuses on the influence of various operating parameters, such as pressure, temperature, and the inclusion of a cosolvent, on the solubility of NHM in $scCO_2$. Several density models, including those proposed by Méndez-Santiago and Teja (MS·T)[70], Sodeifian-Sajadian[66], Soltani-Mazloumi[65], González et al.[71], Jouyban et al.[62], and Garlapati-Madras[63], were used to correlate the solubility data of NHM for this ternary system. The parameters of these models were determined. Finally, the average absolute relative deviation (AARD%) and the adjusted correlation coefficient (R_{adj}) were used to ponder the accuracy of the model predictions.

Materials and methods

In this section, the list and properties of the various materials used in the experiments are presented. Also, the experimental apparatus and the experimental procedures are described in detail. Finally, the calculation procedures are laid out.

Materials

The key compound used in this work is nilotinib hydrochloride monohydrate (form B), obtained from Tofigh Daru Pharmaceutical Company. The NHM formula is $C_{28}H_{25}ClF_3N_7O_2$ and therefore its molar mass is 584.0 g/mol. The NHM structure is shown in Fig. 1, which is the nilotinib (plain) plus the HCl group (monohydrochloride) and the water group (monohydrate). Additionally, the source and purity of carbon dioxide and ethanol, that were also used, are displayed in Table 1.

Experimental setup

The schematic of the laboratory configuration is shown in Fig. 2. Its caption includes the specifications of the various elements therein. The entire assembly of this high-pressure unit, including tubing and fittings, is made of 316 stainless steel. The brand of tubing used is Sandvik, and it has an external diameter of 1/8 inch or 3.18-mm, a thickness of 0.89 mm, and an internal diameter of 1.4-mm.

The laboratory configuration illustrated in Fig. 2 includes a spectrophotometer and various other components, such as CO_2 tank, air compressor (Finac, China), refrigeration unit, high-pressure pump (Haskel type pump, model: MSHP-71, Burbank CA 91502, USA), filter, needle valve, back-pressure regulator (Xi'an Shelok Instrument Technology Co., Ltd.), metering valve (Fitok, MHSS-FL4-V, Germany), equilibrium cell, and oven (Memmert Oven UNB 100, Germany). A manometer (Shllj, LZM-6T) and a transmitter (Wika, EN 837-1) were used to measure and transmit the system pressure.

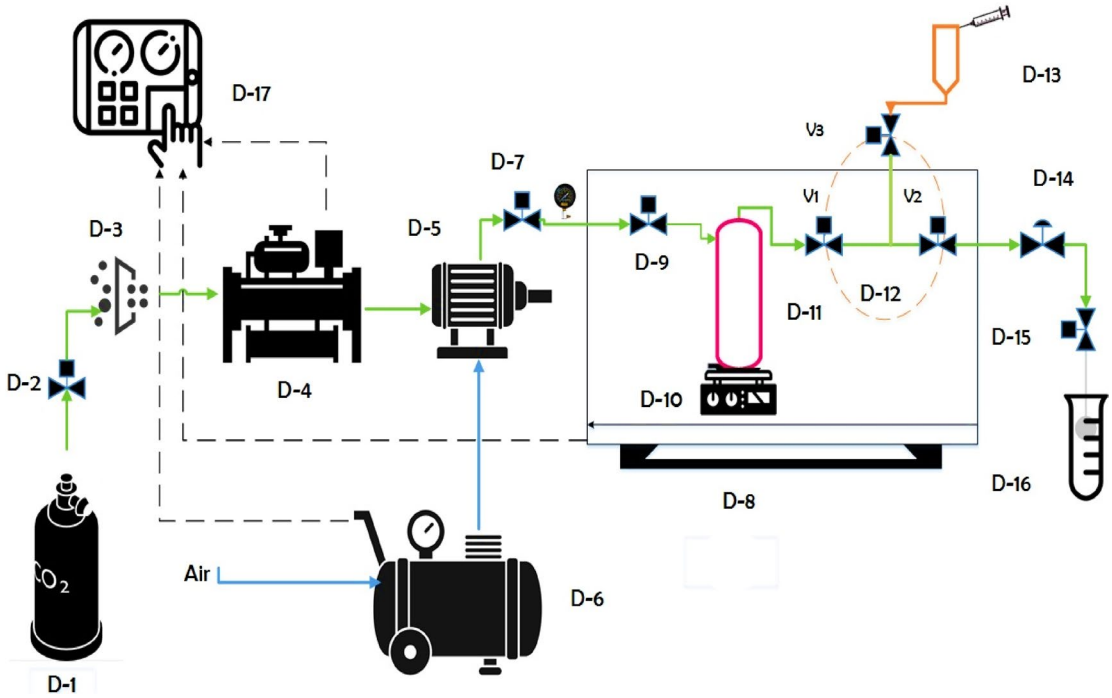

Fig. 2. Experimental setup. D-1: CO_2 Tank, D-2: needle valve, D-3: filter, D-4: refrigerator unit, D-5: high-pressure pump, D-6: compressor, D-7: needle valve, D-8: oven, D-9: needle valve, D-10: magnetic stirrer, D-11: equilibrium cell, D-12: loop, D-13: syringe, D-14: back-pressure regulator, D-15: metering valve, D-16: collection vial, D-17: panel, and V_1, V_2, and V_3: valves.

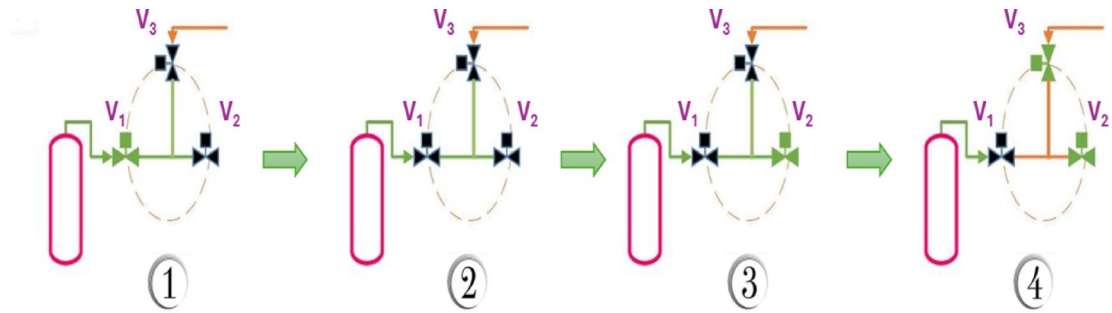

Fig. 3. Sequence steps in sampling. (Green means valve is open; black means it is closed.)

Experimental procedure

The CO_2 was purified by passing it through a filter (D-3 in Fig. 2). Subsequently, due to the low internal temperature, CO_2 liquefied in the refrigeration system (-5°C). Liquid CO_2 was then drawn into the high-pressure pump (approximately 6 MPa) from the CO_2 tank. The system pressure was monitored and recorded with an accuracy of 0.1 MPa.

The NHM was placed into a 300-mL cell, where a magnetic stirrer was used to ensure the solution was well-mixed in $scCO_2$. The pressure within the equilibrium cell was adjusted to the desired level using compressed CO_2. Once the necessary pressure and temperature were attained, the cell was maintained in that state to reach equilibrium. For the ternary system, CO_2 containing 3.0% (mol basis) of ethanol was added to the cell along with 3000 mg (3 g) of the NHM. Ethanol was inserted directly into the cell. The calculation details for value of ethanol in each experiment have been included in the supplementary file (Table S1). An oven was used to control the temperature throughout the process. A sintered filter was positioned on either side of the cell to secure the NHM. Prior to introducing the CO_2 into the cell, it was compressed to the appropriate pressure. Initial tests revealed that a static time of 135 min was sufficient to reach equilibrium. After this period, a three-valve device (V_1-V_3) with two positions was used to fill the injection loop with saturated $scCO_2$ (300 µL ± 0.3 µL). Following the rerouting of the injection valve, the loop was placed into the collecting vial to retain a specific volume (4 mL) of ethanol (solvent). This method is summarized in the four steps illustrated in Fig. 3.

The static time must precede the filling of the loop. First, valve V_1 is opened {step ①}, and once the loop is filled, valve V_1 is closed {step ②} and valve V_2 is opened {step ③}. After positioning the loop in the collecting vial, V_3 is opened {step ④}, and 1 mL of ethanol is used to rinse both the loop and all connecting lines. The open and closed states of the valves are represented in Fig. 3 by green and black colors, respectively. This procedure was repeated three times (triplicate) for each system and each data point.

The final volume of solution in the collection vial (5 mL ± 0.2%) was collected for next step (UV spectrophotometry). The absorbance was measured at a wavelength of 280 nm that corresponds to a maximum absorbance (λ_{max}). The absorbance was measured using UV spectrophotometry with a Jenway UV instrument equipped with a quartz cell. A calibration curve that showed a linear relationship across a wide range of concentrations (with a regression coefficient of 0.997) was previously determined. The solubility was determined by measuring the solution absorbance and converting that to solubility with the calibration curve.

Data processing and solubility calculation

This section describes the calculation of the solubility at the various temperatures and pressures from the experimental measurements described above. Subscripts 1 and 2 refer here to solvent and solute, respectively. The raw data used in these calculations are the concentration C_2 (expressed as mass/volume) from the spectrometer measurements, the volume of the collection vial V_s, and the volume of the sampling loop, V_L. Other properties (mainly molar mass) of the solute and the solvent (CO_2) are also required. With this information, the mole fractions are obtained as follows:

$$n_1 = \frac{\rho V_L}{M_1} \tag{1}$$

$$n_2 = \frac{C_2 V_s}{M_2} \tag{2}$$

$$y_2 = \frac{n_2}{n_1 + n_2} \tag{3}$$

where 1 refers to the solvent (CO_2) and 2 to the solute (NHM), V_s is the volume of the collection vial, V_L is the volume of the sampling loop, and M_1 and M_2 represent the molar masses of the solvent (CO_2) and the solute (NHM), respectively.

When a cosolvent is used (species 3), then the solubility is calculated by:

$$y_2 = \frac{n_2}{n_1 + n_2 + n_3} \tag{4}$$

Here, n_2 and n_3 are calculated with the respective masses contained in the loop (m_2 and m_3) and the molar masses (M_2 and M_3). For species 2, this is valid for the binary and ternary cases.

Summary of experimental results

As mentioned above, both binary experiments (no cosolvent) and ternary experiments (with ethanol as cosolvent) were carried out. Table 2 displays experimental results of both binary and ternary systems. Also, the last column of the table shows the so-called "magnification factor," "cosolvent enhancement factor (CEF)," or simply "cosolvent effect" (ψ), which represents the ratio of the ternary solubility to the binary solubility at any given condition:

$$\psi = \frac{y_{2,t}}{y_{2,b}} \tag{5}$$

where $y_{2,t}$ is the NHM solubility in the ternary system and $y_{2,b}$ corresponds to that in the binary system at the same temperature and pressure. These results are shown graphically in Fig. 4(a) for the binary system and Fig. 4(b) for the ternary case. Although these figures look similar, note the scale difference of the ordinates (y-axes) in them: 4(a) goes up to 80 PPM while 4(b) goes up to 450 PPM corresponding to a factor of almost 6. This is the order of magnitude of the CEF (or ψ) just defined (Eq. 5).

Another way to visualize the magnitude of the cosolvent effect is by the graphs presented in Fig. 5. The two bottom lines represent the solubility of the drug (NHM) as a function of density at constant temperature. The bottom line (in blue) is for the binary case, while the middle one is for the case in which ethanol is added (ternary case). The left figure (Fig. 5a) is at lowest of the four temperatures studied (308 K) and the right figure (Fig. 5b) is at highest of the four temperatures (338 K). At 308 K, the enhancement factor or cosolvent effect (ψ) is within the rough range of 4 to 6.5 and decreases with temperature. At the highest temperature, ψ is about 6 and 11 meaning the cosolvent effect increases with temperature.

In addition, based on XRD analysis before and after the solubility test, there is no evidence of polymorph conversion for the NHM sample. The information on XRDs has been added to the supplementary file (Figure S1).

Modeling

Several models were used in this work to represent experimental data. To select the models, it was important that the models applied to ternary systems (i.e., systems that included a cosolvent). Therefore, models like Chrastil[72], Sparks et al.[73], Bian et al.[74], and Bartle et al.[18] were not considered since they mostly apply to binary systems

T K	P MPa	Binary			Ternary			
		Density (kg/m^3)	$y_{2,b}$ (PPM)	Uncertainty ×10^6	Density (kg/m^3)	$y_{2,t}$ (PPM)	Uncertainty ×10^7	ψ cosolvent effect
308	12	768.42	10.8	0.08	769.05	69.8	14.82	6.46
	15	816.06	14.4	0.07	815.18	83.4	17.70	5.79
	18	848.87	20	0.10	846.86	99.4	21.05	4.97
	21	874.40	24.8	0.08	871.44	115.2	24.45	4.65
	24	895.54	30.6	0.12	891.76	137.9	29.21	4.51
	27	913.69	38.3	0.06	909.18	160.8	34.17	4.20
	30	929.68	47.7	0.11	924.51	196.5	40.19	4.12
318	12	659.73	5.6	0.10	663.14	42.3	9.51	7.56
	15	743.17	12.4	0.10	744.53	82.4	17.61	6.64
	18	790.18	18	0.20	790.14	107.2	22.92	5.96
	21	823.70	27	0.14	822.57	140.3	29.79	5.20
	24	850.10	35.1	0.20	848.04	168.9	35.97	4.81
	27	872.04	44.7	0.09	869.17	211.3	45.16	4.73
	30	890.92	59.2	0.15	887.33	276.3	56.44	4.67
328	12	506.85	1.5	0.11	512.60	13.8	4.44	9.21
	15	654.94	9.2	0.07	658.45	71.2	15.23	7.74
	18	724.13	15.5	0.23	726.00	92.7	20.38	5.98
	21	768.74	26.8	0.20	769.36	156.2	33.63	5.83
	24	801.92	39.4	0.13	801.51	220.2	47.08	5.59
	27	828.51	53.5	0.17	827.21	288.3	61.30	5.39
	30	850.83	67.4	0.11	848.74	353.7	72.26	5.25
338	12	384.17	1	0.61	390.45	10.8	3.44	10.80
	15	555.23	5.9	0.18	560.44	54.6	12.37	9.26
	18	651.18	12.9	0.14	654.77	110.3	24.31	8.55
	21	709.69	27	0.20	711.93	188.4	40.74	6.98
	24	751.17	47	0.08	752.30	276.4	58.96	5.88
	27	783.29	61	0.14	783.47	351.6	74.57	5.76
	30	809.58	73.6	0.17	808.92	415.2	84.84	5.64

Table 2. Experimental solubility of NHM in $scco_2$ (binary) and in $scco_2$ + 3% ethanol (ternary). [a]Standard uncertainty u are u(T) = 0.1 K; u(p) = 0.1 MPa.

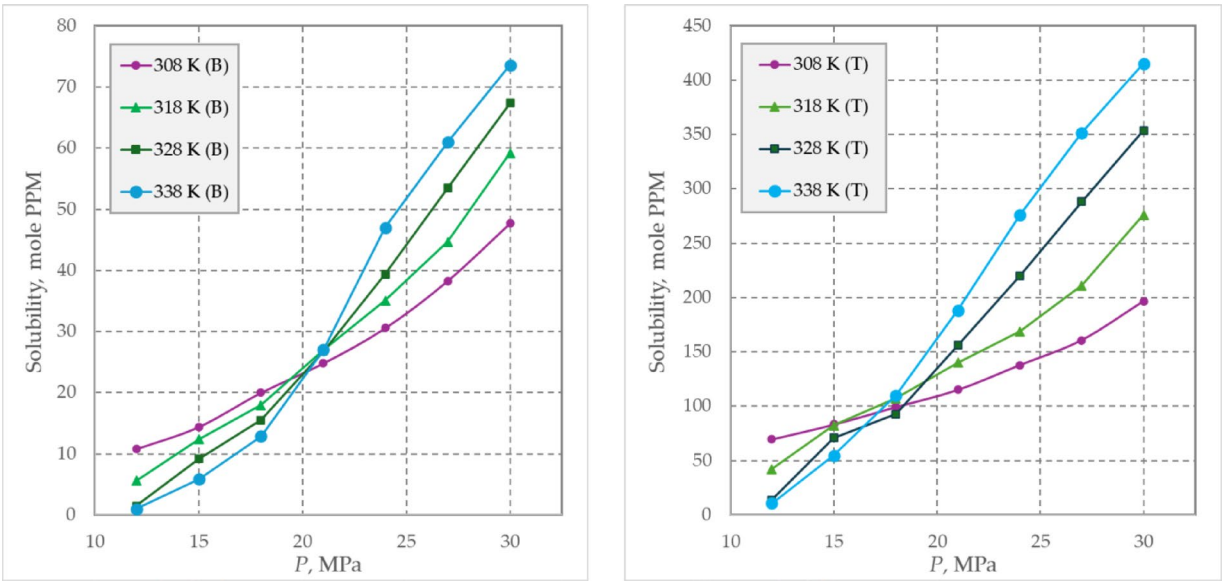

Fig. 4. Experimental solubility (in molar PPM) of NHM in $scCO_2$: Binary system (left) and ternary system (right). Note the *y*-axes scales difference (up to 80 in the binary case vs. 450 in the ternary case; almost a factor of 6). The graphical abstract shows these data on a single, semi log representation.

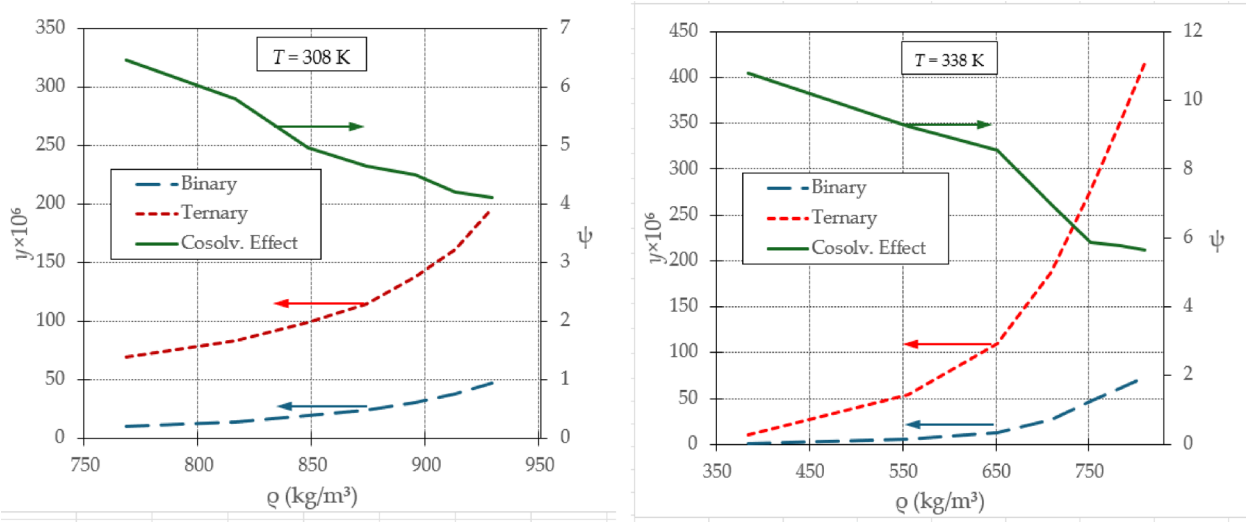

Fig. 5. Isothermal solubilities (expressed as PPM) of NHM as a function of density at constant temperatures (two bottom lines) and cosolvent effect (top line) at 308 K (left) and 338 K (right).

Model	Equation	N_{const}*
Méndez-Santiago & Teja[70]	$T \ln\left(\frac{y_2 P}{P_{ref}}\right) = a_0 + a_1\rho_1 + a_2 T + a_3 y_3$	4
Sodeifian & Sajadian[66]	$\ln(y_2) = \left(a_0 + \frac{a_1\rho_1}{T}\right)\ln\rho_1 + a_2\rho_1 + a_3 \ln(y_3 P)$	4
González et al.[71]	$\ln(y_2) = a_0 \ln(\rho_1) + a_1 \ln(y_3) + \frac{a_2}{T} + a_3$	4
Soltani & Mazloumi[65]	$\ln(y_2) = a_0 + \frac{a_1}{T} + a_2\frac{\rho_1}{T} - a_3 \ln(P) + a_4 \ln(y_3\rho_1 T)$	5
Garlapati & Madras[75]	$\ln(y_2) = a_0 + a_1 \ln(\rho_1) + a_2\rho_1 - \frac{a_3}{T} + a_4 \ln(T) + a_5 \ln(y_3) + a_6 \ln(y_3\rho_1 T)$	7
Jouyban et al.[62]	$\ln(y_2) = a_0 + a_1 y_3 + a_2\rho_1 + a_3 P^2 + a_4 PT + a_5\frac{T}{P} + a_6 \ln(\rho_1)$	7

Table 3. Models used to correlate experimental solubility data. * N_{const} Refers to the number of adjustable parameters (or adjustable constants) in each model.

(no cosolvent). In this contribution, the following six (6) models that apply to ternary systems were selected: Méndez-Santiago and Teja[70], Sodeifian and Sajadian[66], González et al.[71], Soltani and Mazloumi[65], Garlapati and Madras[75], and Jouyban et al.[62]. The corresponding equations are displayed in Table 3. The Méndez-Santiago and Teja[76] is an extension of their binary model by adding the last term, which is a linear dependence on the mole fraction of the cosolvent. The Sodeifian and Sajadian model[77] took some concepts from the González et al. model[71] to modify the Chrastil (binary) model. González et al.[71] discussed the model by Chrastil that combines an exponential relationship between solubility and cosolvent levels with a logarithmic dependence on liquid density. This model effectively estimates solute solubility in non-entrained supercritical liquids, especially when an entrainer significantly enhances solubility through solute-entrainer interactions. It suggests that solute, entrainer, and solvent form clusters or solvate complexes, aligning with observations that temperature negatively impacts solute solubility. However, the model may not accurately predict solubility in systems where the cosolvent only acts as cosolvent for CO_2 without exhibiting the entrainer effect that boosts solubility. The Soltani and Mazloumi model[65] is a newly developed five-parameter model that is used to predict the solubility of solids in $scCO_2$ in the presence of a cosolvent. This model is based on the relationship between density, pressure, temperature, and other relevant input factors. It is based on the work of Hozhabr et al.[78] and features three primary relations: a linear one between ln y_2 and ln y_3, a nonlinear relationship between ln y_2 and both temperature and density, and a linear correlation between ln y_2 and ln y_3. The Garlapati and Madras equation[63], developed in 2010 and based on Jouyban et al. model, and uses seven adjustable constants to relate the solubility of high-molar-mass substances in $scCO_2$ to temperature, $scCO_2$ density, and cosolvent mole fraction. It can be applied to binary or ternary systems (i.e., with or without cosolvent).

The adjustable parameters in each model were obtained by regression of the experimental data. To this end, the simulated annealing algorithm in MATLAB software was used to estimate adjustable parameters. AARD was used to assess the model's performance.

Model	a_0	a_1	a_2	a_3	a_4	a_5	a_6
MS·T	-8720.6	3.74	22.25	-8472.8	—	—	—
Sodeifian & Sajadian	-3.053	-1.046	0.0363	0.1644	—	—	—
González et al.	5.986	-7.78	-591.33	-57.67	—	—	—
Soltani & Mazloumi	15.42	9660.31	3.19	0.259	-0.152	—	—
Garlapati & Madras	52.65	-13.49	0.0058	-328.27	2.736	35.71	15.02
Jouyban et al.	-40.51	0.41	-0.00057	-0.0058	0.00125	0.1204	3.644

Table 4. Coefficients of the models listed in Table 3.

Model	Param.	AARD%	R_{adj}
MS·T	4	*9.202*	0.988
Sodeifian & Sajadian	4	10.570	0.990
González et al.	4	10.520	0.990
Soltani & Mazloumi	5	9.370	*0.993*
Garlapati & Madras	7	9.810	0.985
Jouyban et al.	7	13.280	0.988

Table 5. *AARD*% and R_{adj} for the models listed in Table 4.

$$AARD\% = \frac{100}{N-Z}\sum_{i=1}^{N}\frac{\left|y_2^{calc}-y_2^{\exp}\right|}{y_2^{\exp}} \tag{6}$$

The correlation coefficient R^2 was used to compare the various models, and it is defined by:

$$R^2 = 1-\frac{SS_E}{SS_T} = 1-\frac{\sum_{i=1}^{N}\left(y_2^{\exp}-y_2^{calc}\right)^2}{\sum_{i=1}^{N}\left(y_2^{\exp}\right)^2-\frac{1}{N}\sum_{i=1}^{N}\left(y_2^{calc}\right)^2} \tag{7}$$

where SS_E represents the sum square error and SS_T denotes the total sum of squares[79,80]. On the other hand, the numbers in any set or model are the subject of the information, while Z and N_i stand for the changeable parameter numbers for each presentation[27]. R_{adj} was used when comparing various models[63,80,81]:

$$R_{adj} = \sqrt{\left|R^2-\frac{Q\left(1-R^2\right)}{N-Q-1}\right|} \tag{8}$$

Finding and outcomes

Modeling results

The solubility of NHM in $scCO_2$ + ethanol (cosolvent) was experimentally determined at four temperatures between 308 K and 338 K and six pressures between 12 and 30 MPa, as reported in Table 2. The $scCO_2$ densities in the binary and ternary systems reported in Table 2 were calculated using the Span-Wagner EoS[82,83]. The experimental data were correlated with temperature, pressure, and density as "independent variables." Note that, mathematically, there are only two independent variables, as the density is a function of temperature and pressure. However, density is used as an "independent" variable for physical reasons since the solubility is known to be a strong function of the density of de SCF. Table 4 shows the constants for the models listed in Table 3. Statistical indicators of the goodness of the fittings (*AARD*% and R_{adj}) are reported in Table 5 keeping the same order of the models used in Table 4 (from fewer constants on).

Interestingly, the best *AARD*% (lowest value) corresponds to the MST model with just four adjustable parameters. Similarly, the best R_{adj} corresponds to the Soltani & Mazloumi, which has just 5 adjustable parameters. (The best value in each of the last two columns is in *italics*, in Table 5). The last two models, that have seven adjustable parameters, have the worst R_{adj} of all models, and ranked third and last in terms of *AARD*%.

Furthermore, the self-consistency of the experimental solubility data of NHM was tested using MSTs for binary and ternary solubility, as illustrated in Figure S2. As can be seen, the model correlation line and the experimental solubility data confirm the self-consistency of the data at all temperatures.

In Chrastil's theoretical framework, the dissolution process is modeled as a two-step mechanism. Initially, the solid solute undergoes sublimation, which Chrastil refers to as vaporization. Then, the solute becomes solvated in the solvent. Consequently, the total enthalpy of dissolution is expressed as follows:

$$\Delta H_{diss} = \Delta H_{vap} + \Delta H_{solv} \tag{9}$$

Chrastil equation adjustable parameters are a_0, a_1, and a_2:

$$c = d^{a_0} exp\left(\frac{a_1}{T} + a_2\right) \tag{10}$$

Here, parameter a_1 represents the enthalpy of dissolution, often referred to as total heat (ΔH_{diss}). Through regression analysis of solubility data using Eq. (10), the enthalpy of dissolution was calculated to be 48.01 kJ/mol. According to the Bartle et al. model, the enthalpy of sublimation (ΔH_{vap}) was determined to be 67.35 kJ/mol. In addition, the values of enthalpy of solvation (ΔH_{sol}). (–19.33 [kJ/mol]) was determined as the difference between the ΔH_{vap} (67.35 [kJ/mol]) and ΔH_{total} (48.01 [kJ/mol])[5].

The impact of cosolvent on the solubility

The solubility of NHM in terms of density and pressure at various temperatures is illustrated in Fig. 6(a) to (f) for ternary systems. In 2023, Estévez et al.. conducted research on the NHM in binary mode[5] and observed that the NHM solubility in $scCO_2$ at constant temperature for both systems generally increase with increasing pressure because it increases the solvating power of $scCO_2$ density. That trend is also observed in the ternary case with ethanol as cosolvent. However, the absolute magnitude of solubility is dramatically augmented. To emphasize this, Fig. 7(a) and (b) have been prepared.

Interestingly, the enhancement effect, as quantified by the enhancement factor, ψ, is more pronounced at lower pressures, which could be counterintuitive. The explanation of that could be in Fig. 7(b). Interestingly, the effect of temperature in Fig. 7(b) is almost negligible as all four isotherms seem to be superimposed. That means that the enhancement factor is a weak function of temperature or pressure and a strong function of density. This is not noted in Fig. 7(a) because the density appears indirectly through the temperature and pressure. To emphasize this idea, Fig. 8 was prepared. This figure has the same data as Fig. 7(b), except that it is not segregated by temperature.

Our analysis of NHM's solubility in both binary and ternary systems clearly indicates that the inclusion of a cosolvent, specifically ethanol, significantly improves NHM's solubility in the SCF. Ethanol is recognized as safe for food-related applications, making it a suitable choice for cosolvent use[48]. The data reveals that the cosolvent effects reach a maximum of 10.08 at 338 K and 12 MPa, and a minimum of 4.12 at 308 K and 30 MPa, as observed in Fig. 8. Note that the solubility enhancement (ψ) quantifies the effect of adding ethanol as a cosolvent on NHM's solubility in $scCO_2$[43,72].

Conclusions

This work investigates the solubility of nilotinib hydrochloride monohydrate in a supercritical fluid system, within the temperature range of 308 K to 338 K and pressures from 12 MPa to 30 MPa, utilizing $scCO_2$ with ethanol as a cosolvent. The solubilities for the ternary system were between 0.108×10^{-4} and 4.15×10^{-4} (10.8 to 415 PPM). Adding ethanol as a cosolvent greatly improved the solubility of nilotinib hydrochloride monohydrate, which is attributed to the intermolecular connections between the compound's dipoles and the cosolvent. The data supported this conclusion, with the highest cosolvent enhancement factor (ψ) of 10.80 at 338 K and 12 MPa. Within the specified temperature and pressure conditions, the highest solubility of nilotinib hydrochloride monohydrate observed in the presence of ethanol as cosolvent was 4.152×10^{-4} (415.2 PPM). Additionally, González et al. showed the strongest correlation of the data for this ternary system.

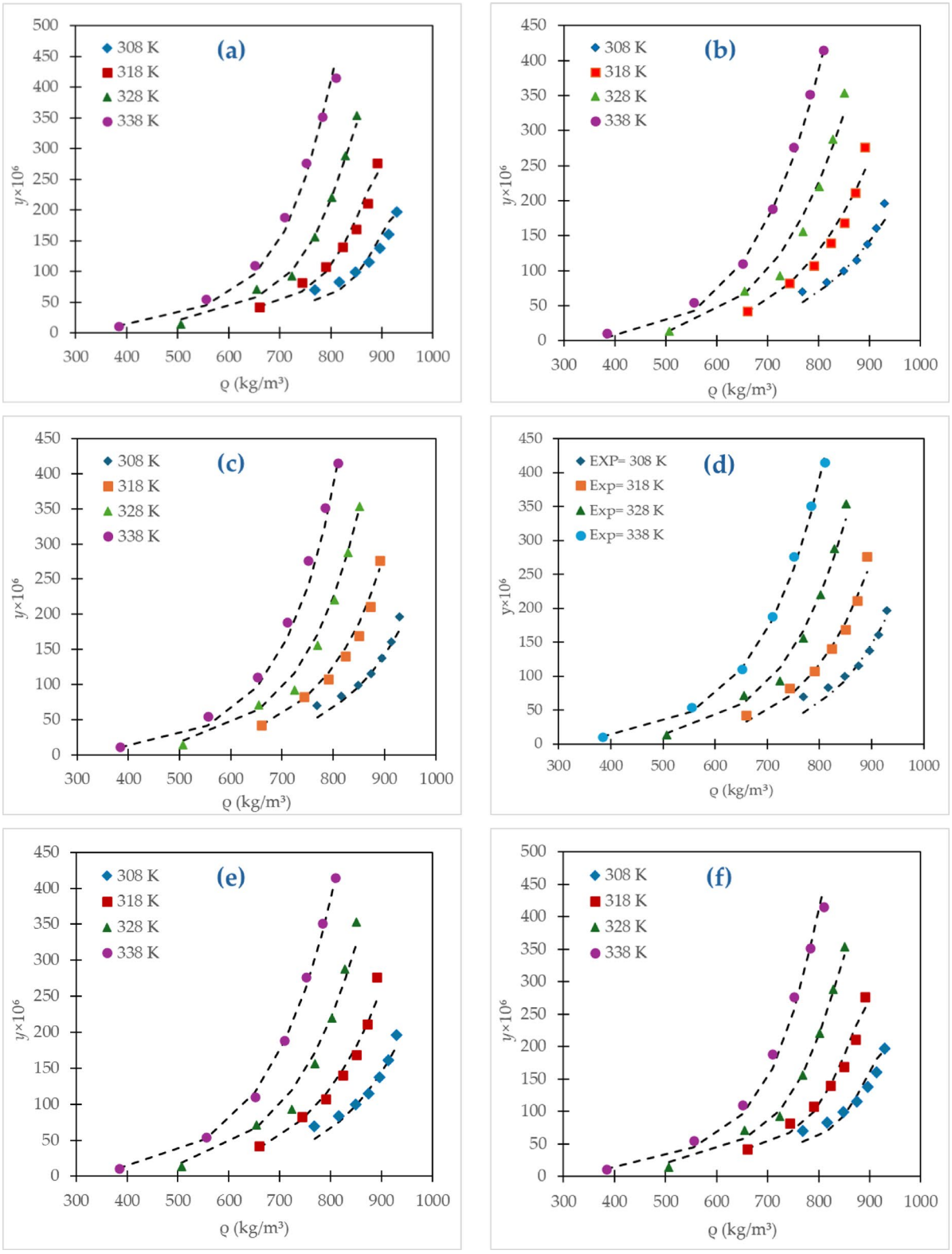

Fig. 6. Solubility (as PPM, mole basis) of NHM in $scCO_2$ (symbols are experimental data and lines show modeling results): **(a)** Méndez-Santiago and Teja (top-left); **(b)** Sodeifian & Sajadian; **(c)** González et al.; **(d)** Soltani & Mazloumi; **(e)** Garlapati & Madras; **(f)** Jouyban et al.

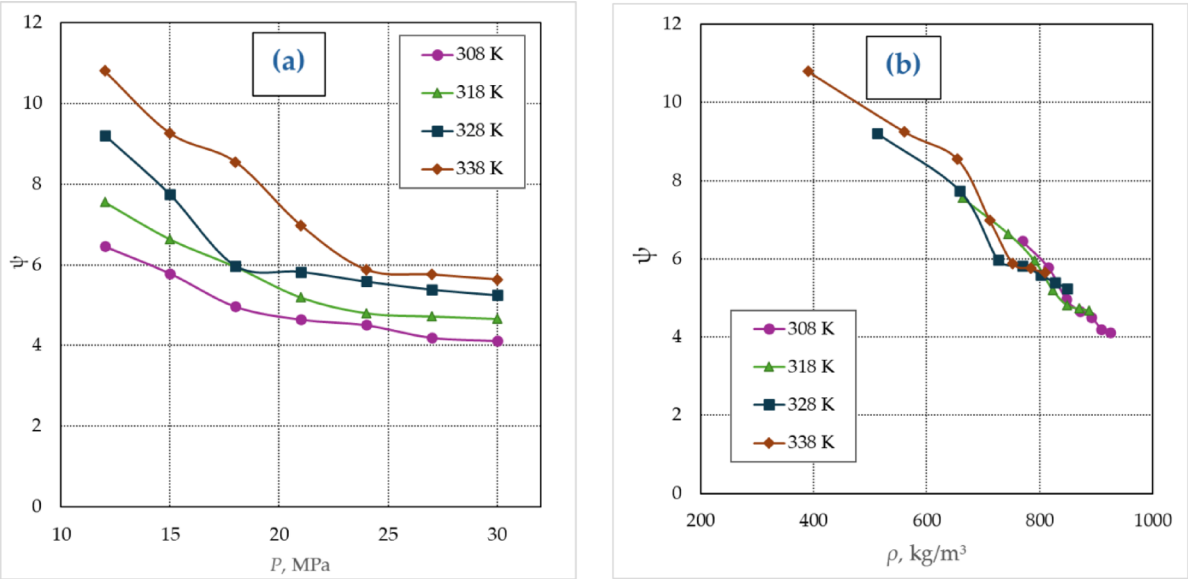

Fig. 7. Cosolvent enhancement factor, ψ, of NHM in $scCO_2$ (symbols are experimental data and lines show trends): **(a)** Cosolvent effect vs. pressure; **(b)** Cosolvent effect vs. density.

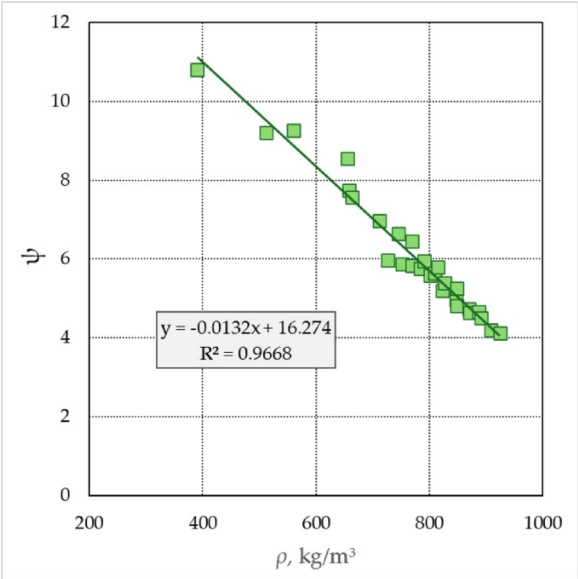

Fig. 8. Cosolvent enhancement factor, ψ, vs. density including all the data without discriminating them by temperature.

Data availability

All data generated or analysed during this study are included in this published article.

Received: 31 May 2025; Accepted: 11 September 2025
Published online: 05 October 2025

References

1. Herbrink, M., Schellens, J. H. M., Beijnen, J. H. & Nuijen, B. Improving the solubility of nilotinib through novel spray-dried solid dispersions. *Int. J. Pharm.* **529**, 294–302. https://doi.org/10.1016/j.ijpharm.2017.07.010 (2017).
2. Sasaki, M., Aoyama, T., Sugawara, M. & Takekuma, Y. Influence of Gastrointestinal activity on the absorption of nilotinib. *Drug Metab. Pharmacokinet.* **35**, 102–110. https://doi.org/10.1016/j.dmpk.2019.08.006 (2020).
3. Pursche, S., Ottmann, O. G., Ehninger, G. & Schleyer, E. High-performance liquid chromatography method with ultraviolet detection for the quantification of the BCR-ABL inhibitor nilotinib (AMN107) in plasma, urine, culture medium and cell preparations. *J. Chromatogr. B.* **852**, 208–216. https://doi.org/10.1016/j.jchromb.2007.01.019 (2007).

4. Hazarika, M. et al. Tasigna for chronic and accelerated phase Philadelphia chromosome–positive chronic myelogenous leukemia resistant to or intolerant of Imatinib. *Clin. Cancer Res.* **14**, 5325–5331. https://doi.org/10.1158/1078-0432.CCR-08-0308 (2008).
5. Estévez, L. A., Sajadian, S. A., Askarizadeh, M. & Honarvar, B. *Measurement and Modeling of the Solubility of Nilotinib Monohydrochloride Monohydrate in Supercritical Carbon Dioxide*. https://doi.org/10.2139/ssrn.4516325.
6. Imran, M. et al. Innovations and patent trends in the development of USFDA approved protein kinase inhibitors in the last two decades. *J. Pharm.* **14**, 710. https://doi.org/10.3390/ph14080710 (2021).
7. Kim, T. D. & Dörken, B. Le coutre; nilotinib for the treatment of chronic myeloid leukemia. *Expert Rev. Hematol.* **1**, 29–39. https://doi.org/10.1586/17474086.1.1.29 (2008).
8. Ribeiro, N. et al. A new era for sterilization based on supercritical CO2 technology. *J. Biomed. Mater. Res. B Appl. Biomater.* **108**, 399–428. https://doi.org/10.1002/jbm.b.34398 (2020).
9. Belghait, A., Si-Moussa, C., Laidi, M. & Hanini, S. Semi-empirical correlation of solid solute solubility in supercritical carbon dioxide: comparative study and proposition of a novel density-based model. *C R Chim.* **21**, 494–513. https://doi.org/10.1016/j.crci.2018.02.006 (2018).
10. Esfandiari, N. & Sajadian, S. A. CO2 utilization as gas antisolvent for the pharmaceutical micro and nanoparticle production: A review. *Arab. J. Chem.* 104164. https://doi.org/10.1016/j.arabjc.2022.104164 (2022).
11. Zhang, M., Dou, M., Wang, M. & Yu, Y. Study on the solubility parameter of supercritical carbon dioxide system by molecular dynamics simulation. *J. Mol. Liq.* **248**, 322–329. https://doi.org/10.1016/j.molliq.2017.10.056 (2017).
12. Askarizadeh, M., Esfandiari, N., Honarvar, B., Sajadian, S. A. & Azdarpour, A. Kinetic modeling to explain the release of medicine from drug delivery systems. *ChemBioEng Rev.* **10**, 1006–1049. https://doi.org/10.1002/cben.202300027 (2023).
13. Dohrn, R., Fonseca, J. M. & Peper, S. Experimental methods for phase equilibria at high pressures. *Annu. Rev. Chem. Biomol. Eng.* **3**, 343–367. https://doi.org/10.1146/annurev-chembioeng-062011-081008 (2012).
14. Sajadian, S. A., Esfandiari, N. & Padrela, L. CO2 utilization as a gas antisolvent in the production of Glibenclamide nanoparticles, Glibenclamide-HPMC, and Glibenclamide-PVP composites. *J. CO2 Util.* **84**, 102832. https://doi.org/10.1016/j.jcou.2024.102832 (2024).
15. Park, H. et al. Pharmaceutical applications of supercritical fluid extraction of emulsions for micro-/nanoparticle formation. *Pharm* **13**, p1928. https://doi.org/10.3390/pharmaceutics13111928 (2021).
16. KravanjaK.A., Finšgar, M., Knez, Ž. & Knez Marevci, M. Supercritical fluid technologies for the incorporation of synthetic and natural active compounds into materials for drug formulation and delivery. *Pharm* **14**, 1670. https://doi.org/10.3390/pharmaceutics14081670 (2022).
17. Kankala, R. K., Zhang, Y. S., Wang, S. B., Lee, C. H. & Chen, A. Z. Supercritical fluid technology: an emphasis on drug delivery and related biomedical applications. *Adv. Healthc. Mater.* **6**, p1700433. https://doi.org/10.1002/adhm.201700433 (2017).
18. Bartle, K., Clifford, A., Jafar, S. & Shilstone, G. Solubilities of solids and liquids of low volatility in supercritical carbon dioxide. *J. Phys. Chem. Ref. Data*. **20**, 713–756. https://doi.org/10.1063/1.555893 (1991).
19. Johannsen, M. & Brunner, G. Solubilities of the fat-soluble vitamins A, D, E, and K in supercritical carbon dioxide. *J. Chem. Eng. Data*. **42**, 106–111. https://doi.org/10.1021/je960219m (1997).
20. Aionicesei, E., Škerget, M. & Knez, Ž. Measurement of CO2 solubility and diffusivity in Poly (l-lactide) and Poly (d, l-lactide-co-glycolide) by magnetic suspension balance. *J. Supercrit Fluids*. **47**, 296–301. https://doi.org/10.1016/j.supflu.2008.07.011 (2008).
21. Asiabi, H., Yamini, Y., Latifeh, F. & Vatanara, A. Solubilities of four macrolide antibiotics in supercritical carbon dioxide and their correlations using semi-empirical models. *J. Supercrit Fluids*. **104**, 62–69. https://doi.org/10.1016/j.supflu.2015.05.018 (2015).
22. Sodeifian, G., Sajadian, S. A. & Razmimanesh, F. Solubility of an antiarrhythmic drug (amiodarone hydrochloride) in supercritical carbon dioxide: experimental and modeling. *Fluid Ph Equilib.* **450**, 149–159. https://doi.org/10.1016/j.fluid.2017.07.015 (2017).
23. Bin, L. K. et al. Supercritical fluid technology and its pharmaceutical applications: A revisit with two decades of progress. *Indian J. Pharm. Educ. Res.* **54**, s1–s3. https://doi.org/10.5530/ijper.54.2s.56 (2020).
24. Savjani, K. T., Gajjar, A. K. & Savjani, J. K. Drug solubility: importance and enhancement techniques. *Int. Sch. Res. Notices* **2012**. https://doi.org/10.5402/2012/195727 (2012).
25. Guptaa, S. K., Guptaa, R. K., Pandeya, N. K., Singha, S. K. & Kumara, B. *Solubility Enhancement Techniques: A Comparative Study* (2018).
26. Thapa, R. K., Choi, H. G., Kim, J. O. & Yong, C. S. Analysis and optimization of drug solubility to improve pharmacokinetics. *J. Pharm. Investig.* **47**, 95–110. https://doi.org/10.1007/s40005-016-0299-z (2017).
27. Sajadian, S. A., Ardestani, N. S., Esfandiari, N., Askarizadeh, M. & Jouyban, A. Solubility of favipiravir (as an anti-COVID-19) in supercritical carbon dioxide: An experimental analysis and thermodynamic modeling. *J. Supercrit. Fluids* **183**, 105539. https://doi.org/10.1016/j.supflu.2022.105539 (2022).
28. Dohrn, R., Peper, S., Secuianu, C. & Fonseca, J. M. S. High-pressure fluid-phase equilibria: experimental methods, developments and systems investigated (2013–2016). *Fluid Ph Equilib.* **579**, 113978. https://doi.org/10.1016/j.fluid.2023.113978 (2024).
29. MacEachern, L., Kermanshahi-pour, A. & Mirmehrabi, M. Supercritical carbon dioxide for pharmaceutical co-crystal production. *Cryst. Growth Des.* **20**, 6226–6244. https://doi.org/10.1021/acs.cgd.0c00571 (2020).
30. Pishnamazi, M. et al. Measuring solubility of a chemotherapy-anti cancer drug (busulfan) in supercritical carbon dioxide. *J. Mol. Liq.* **317**, 113954. https://doi.org/10.1016/j.molliq.2020.113954 (2020).
31. Pishnamazi, M. et al. Using static method to measure Tolmetin solubility at different pressures and temperatures in supercritical carbon dioxide. *Sci. Rep.* **10**, 1–7. https://doi.org/10.1038/s41598-020-76330-9 (2020).
32. Pishnamazi, M. et al. Shirazian; chloroquine (antimalaria medication with anti SARS-CoV activity) solubility in supercritical carbon dioxide. *J. Mol. Liq.* **322**, 114539. https://doi.org/10.1016/j.molliq.2020.114539 (2021).
33. Cheng, J., Han, S., Song, J., Wang, W. & Jiao, Z. Solubility of vitamin E acetate in supercritical carbon dioxide with ethanol as cosolvent. *J. Chem. Eng. Data*. **63**, 4248–4255. https://doi.org/10.1021/acs.jced.8b00745 (2018).
34. Esfandiari, N. & Ghoreishi, S. M. Synthesis of 5-fluorouracil nanoparticles via supercritical gas antisolvent process. *J. Supercrit Fluids*. **84**, 205–210. https://doi.org/10.1016/j.supflu.2013.10.008 (2013).
35. Esfandiari, N. Production of micro and nano particles of pharmaceutical by supercritical carbon dioxide. *J. Supercrit Fluids*. **100**, 129–141. https://doi.org/10.1016/j.supflu.2014.12.028 (2015).
36. Esfandiari, N. & Ghoreishi, S. M. Ampicillin nanoparticles production via supercritical CO2 gas antisolvent process. *Aaps Pharmscitech* **16**, 1263–1269. https://doi.org/10.1208/s12249-014-0264-y (2015).
37. Najafi, M., Esfandiari, N., Honarvar, B. & Aboosadi, Z. A. Production of Rosuvastatin calcium nanoparticles using gas antisolvent technique: experimental and optimization. *Period Polytech. Chem. Eng.* **65**, 442–453. https://doi.org/10.3311/PPch.16629 (2021).
38. Rojas, A., Sajadian, S. A., Razmimanesh, F., Aguila, G. & Esfandiari, N. Jouyban; solubility of Oxazepam in supercritical carbon dioxide: experimental and modeling. *Fluid Ph Equilib.* **585**, 114165. https://doi.org/10.1016/j.fluid.2024.114165 (2024).
39. Bazaei, M., Honarvar, B., Esfandiari, N., Sajadian, S. A. & Arab Aboosadi, Z. Preparation of erlotinib hydrochloride nanoparticles (anti-cancer drug) by RESS-C method and investigating the effective parameters. *Sci. Rep.* **14**, p14955. https://doi.org/10.1038/s41598-024-64477-8 (2024).
40. Ardestani, N. S., Sajadian, S. A., Esfandiari, N., Rojas, A. & Garlapati, C. Experimental and modeling of solubility of sitagliptin phosphate, in supercritical carbon dioxide: proposing a new association model. *Sci. Rep.* **13**, 17506. https://doi.org/10.1038/s41598-023-44787-z (2023).
41. Esfandiari, N. & Sajadian, S. A. Experimental and modeling investigation of Glibenclamide solubility in supercritical carbon dioxide. *Fluid Ph Equilib.* **556**, p113408. https://doi.org/10.1016/j.fluid.2022.113408 (2022).

42. Behjati Rad, H., Karimi Sabet, J. & Varaminian, F. Effect of stearic acid as a Co-solvent on the solubility enhancement of aspirin in supercritical CO2. *Chem. Eng. Technol.* **42**, 1259–1267. https://doi.org/10.1002/ceat.201900043 (2019).
43. Bitencourt, R. G., Palma, A. M., Coutinho, J. A., Cabral, F. A. & Meirelles, A. J. Prediction of solid solute solubility in supercritical CO2 with cosolvents using the CPA EoS. *Fluid Ph Equilib.* **482**, 1–10. https://doi.org/10.1016/j.fluid.2018.10.020 (2019).
44. Hosseini, S. Z., Bozorgmehr, M. R., Masrurnia, M. & Beyramabadi, S. A. Study of the effects of methanol, ethanol and propanol alcohols as co-solvents on the interaction of methimazole, propranolol and phenazopyridine with carbon dioxide in supercritical conditions by molecular dynamics. *J. Supercrit Fluids*. **140**, 91–100. https://doi.org/10.1016/j.supflu.2018.06.005 (2018).
45. Sodeifian, G., Sajadian, S. A., Razmimanesh, F. & Hazaveie, S. M. Solubility of ketoconazole (antifungal drug) in SC-CO2 for binary and ternary systems: measurements and empirical correlations. *Sci. Rep.* **11**, 1–13. https://doi.org/10.1038/s41598-021-87243-6 (2021).
46. Skerget, M., Knez, Z. & Knez-Hrncic, M. Solubility of solids in sub-and supercritical fluids: a review. *J. Chem. Eng. Data*. **56**, 694–719. https://doi.org/10.1021/je1011373 (2011).
47. Knez, Z. & Cör, D. Knez hrnčič; solubility of solids in sub-and supercritical fluids: a review 2010–2017. *J. Chem. Eng. Data*. **63**, 860–884. https://doi.org/10.1021/acs.jced.7b00778 (2017).
48. Alwi, R.S. et al. Experimental study and thermodynamic modeling of clonazepam solubility in supercritical carbon dioxide. *Fluid Ph Equilib.* **574**, p113880. https://doi.org/10.1016/j.fluid.2023.113880 (2023).
49. Caço, A. I. et al. Solubility of antibiotics in different solvents. Part II. Non-hydrochloride forms of Tetracycline and Ciprofloxacin. *Ind. Eng. Chem. Res.* **47**, 8083–8089. https://doi.org/10.1021/ie8003495 (2008).
50. Zhan, S., Miao, H., Zhao, Y., Wang, J. & Li, Z. Experimental determination and association model for the solubility of laminarin in supercritical carbon dioxide. *J. Chem. Eng. Data*. **65**, 1814–1823. https://doi.org/10.1021/acs.jced.9b01084 (2020).
51. Sajadian, S. A., Peyrovedin, H., Zomorodian, K. & Khorram, M. Using the supercritical carbon dioxide as the solvent of nystatin: studying the effect of co-solvent, experimental and correlating. *J. Supercrit Fluids*. **194**, 105858. https://doi.org/10.1016/j.supflu.2023.105858 (2023).
52. Güçlü-Üstündağ, Ö. & Temelli, F. Solubility behavior of ternary systems of lipids, cosolvents and supercritical carbon dioxide and processing aspects. *J. Supercrit Fluids*. **36**, 1–15. https://doi.org/10.1016/j.supflu.2005.03.002 (2005).
53. Peyrovedin, H. & Shariati, A. Polar Hard-Core Exponential-6 intermolecular potential function for determining the thermodynamic properties of Polar gases. *Ind. Eng. Chem. Res.* **59**, 14106–14114. https://doi.org/10.1021/acs.iecr.0c01465 (2020).
54. Prausnitz, J., Lichtenthaler, R. & Azevedo, E. *Molecular Thermodynamics of Fluid Phase Equilibria*, 3rd edn (Prentice Hall, 1999).
55. Matin, M. M., Uzzaman, M., Chowdhury, S. A. & Bhuiyan, M. M. H. In vitro antimicrobial, physicochemical, pharmacokinetics and molecular Docking studies of benzoyl uridine esters against SARS-CoV-2 main protease. *J. Biomol. Struct. Dyn.* **40**, 3668–3680. https://doi.org/10.1080/07391102.2020.1850358 (2022).
56. Pitchaiah, K., Lamba, N., Sivaraman, N. & Madras, G. Solubility of trioctylmethylammonium chloride in supercritical carbon dioxide and the influence of co-solvents on the solubility behavior. *J. Supercrit Fluids*. **138**, 102–114. https://doi.org/10.1016/j.supflu.2018.04.002 (2018).
57. Cui, C. L., Shi, W. & Long, J. J. Solubility and data correlation of a reactive disperse dye in a quaternary system of supercritical carbon dioxide with mixed cosolvents. *J. Taiwan. Inst. Chem. Eng.* **91**, 213–223. https://doi.org/10.1016/j.jtice.2018.06.028 (2018).
58. Li, G., Zhou, D., Xu, Q. Q., Qiao, G. Y. & Yin, J. Z. Solubility of [bmim]onic liquid [Bmim] ac [bmim]n supercritical CO2 containing different cosolvents. *J. Chem. Eng. Data*. **63**, 1596–1602. https://doi.org/10.1021/acs.jced.7b01108 (2018).
59. Gupta, R. B., Combes, J. R. & Johnston, K. P. Solvent effect on hydrogen bonding in supercritical fluids. *J. Phys. Chem.* **97**, 707–715. https://doi.org/10.1021/j100105a029 (1993).
60. Manna, L. & Banchero, M. Solubility of cortisone and hydrocortisone in supercritical carbon dioxide and ethanol. *J. Chem. Eng. Data*. **68**, 601–611. https://doi.org/10.1021/acs.jced.2c00690 (2023).
61. Reddy, S. N. & Madras, G. Modeling of ternary solubilities of solids in supercritical carbon dioxide in the presence of cosolvents or cosolutes. *J. Supercrit Fluids*. **63**, 105–114. https://doi.org/10.1016/j.supflu.2011.11.016 (2012).
62. Jouyban, A., Chan, H. K. & Foster, N. R. Mathematical representation of solute solubility in supercritical carbon dioxide using empirical expressions. *J. Supercrit Fluids*. **24**, 19–35. https://doi.org/10.1016/S0896-8446(02)00015-3 (2002).
63. Garlapati, C. & Madras, G. New empirical expressions to correlate solubilities of solids in supercritical carbon dioxide. *Thermochim Acta*. **500**, 123–127. https://doi.org/10.1016/j.tca.2009.12.004 (2010).
64. Sajadian, S. A. et al. Mesalazine solubility in supercritical carbon dioxide with and without cosolvent and modeling. *Sci. Rep.* **15**, 3870. https://doi.org/10.1038/s41598-025-86004-z (2025).
65. Soltani, S. & Mazloumi, S. H. A new empirical model to correlate solute solubility in supercritical carbon dioxide in presence of co-solvent. *Chem. Eng. Res. Des.* **125**, 79–87. https://doi.org/10.1016/j.cherd.2017.07.006 (2017).
66. Sodeifian, G., Hazaveie, S. M., Sajadian, S. A. & Razmimanesh, F. Experimental investigation and modeling of the solubility of oxcarbazepine (an anticonvulsant agent) in supercritical carbon dioxide. *Fluid Ph Equilib.* **493**, 160–173. https://doi.org/10.1016/j.fluid.2019.04.013 (2019).
67. Sajadian, S. A. et al. Solubility Measurement and Correlation of Alprazolam in Carbon Dioxide with/without Ethanol at Temperatures from 308 to 338 K and Pressures from 120 to 300 bar. *J. Chem. Eng. Data*. **69**, 1718–1730. https://doi.org/10.1021/acs.jced.3c00587 (2024).
68. Askarizadeh, M., Esfandiari, N., Honarvar, B., Sajadian, S. A. & Azdarpour, A. Binary and ternary approach of solubility of rivaroxaban for preparation of developed nano drug using supercritical fluid. *Arab. J. Chem.* 105707. https://doi.org/10.1016/j.arabjc.2024.105707 (2024).
69. Askarizadeh, M., Esfandiari, N., Honarvar, B., Sajadian, S. A. & Azdarpour, A. Solubility of teriflunomide in supercritical carbon dioxide and co-solvent investigation. *Fluid Ph. Equilib.* **590**, 114284. https://doi.org/10.1016/j.fluid.2024.114284 (2025).
70. Méndez-Santiago, J. & Teja, A. S. The solubility of solids in supercritical fluids. *Fluid Ph. Equilib.* **158**, 501–510. https://doi.org/10.1016/S0378-3812(99)00154-5 (1999).
71. González, J. C., Vieytes, M. R., Botana, A. M., Vieites, J. M. & Botana, L. M. Modified mass action law-based model to correlate the solubility of solids and liquids in entrained supercritical carbon dioxide. *J. Chromatogr. A*. **910**, 119–125. https://doi.org/10.1016/s0021-9673(00)01120-1 (2001).
72. Chrastil, J. Solubility of solids and liquids in supercritical gases. *J. Phys. Chem.* **86**, 3016–3021. https://doi.org/10.1021/j100212a041 (1982).
73. Sparks, D. L., Hernandez, R. & Estévez, L. A. Evaluation of density-based models for the solubility of solids in supercritical carbon dioxide and formulation of a new model. *Chem. Eng. Sci.* **63**, 4292–4301. https://doi.org/10.1016/j.ces.2008.05.031 (2008).
74. Bian, X., Du, Z. & Tang, Y. An improved density-based model for the solubility of some compounds in supercritical carbon dioxide. *Thermochim Acta*. **519**, 16–21. https://doi.org/10.1016/j.tca.2011.02.023 (2011).
75. Saadati Ardestani, N., Amani, M. & Moharrery, L. Determination of anthraquinone Violet 3RN solubility in supercritical carbon dioxide with/without co-solvent: experimental data and modeling (empirical and thermodynamic models). *Chem. Eng. Res. Des.* **159**, 529–542. https://doi.org/10.1016/j.cherd.2020.04.026 (2020).
76. Sauceau, M., Letourneau, J. J., Richon, D. & Fages, J. Enhanced density-based models for solid compound solubilities in supercritical carbon dioxide with cosolvents. *Fluid Ph Equilib.* **208**, 99–113. https://doi.org/10.1016/s0378-3812(03)00005-0 (2003).
77. Rojas, A. et al. Improving and measuring the solubility of favipiravir and Montelukast in SC-CO 2 with ethanol projecting their Nanonization. *RSC Adv.* **13**, 34210–34223. https://doi.org/10.1039/d3ra05484e (2023).

78. Hozhabr, S. B., Mazloumi, S. H. & Sargolzaei, J. Correlation of solute solubility in supercritical carbon dioxide using a new empirical equation. *Chem. Eng. Res. Des.* **92**, 2734–2739. https://doi.org/10.1016/j.cherd.2014.01.026 (2014).
79. Sodeifian, G., Razmimanesh, F. & Sajadian, S. A. Solubility measurement of a chemotherapeutic agent (Imatinib mesylate) in supercritical carbon dioxide: assessment of new empirical model. *J. Supercrit Fluids.* **146**, 89–99. https://doi.org/10.1016/j.supflu.2019.01.006 (2019).
80. Sodeifian, G., Detakhsheshpour, R. & Sajadian, S. A. Experimental study and thermodynamic modeling of Esomeprazole (proton-pump inhibitor drug for stomach acid reduction) solubility in supercritical carbon dioxide. *T J. Supercrit Fluids.* **154**, 104606. https://doi.org/10.1016/j.supflu.2019.104606 (2019).
81. Jouyban, A., Rehman, M., Shekunov, B. Y., Chan, H. K. & Clark, B. J. York; solubility prediction in supercritical CO2 using minimum number of experiments. *J. Pharm. Sci.* **91**, 1287–1295. https://doi.org/10.1002/jps.10127 (2002).
82. Span, R. & Wagner, W. A new equation of state for carbon dioxide covering the fluid region from the triple-point temperature to 1100 K at pressures up to 800 MPa. *J. Phys. Chem. Ref. Data*. **25**, 1509–1596. https://doi.org/10.1063/1.555991 (1996).
83. Sodeifian, G. & Sajadian, S. A. Experimental measurement of solubilities of Sertraline hydrochloride in supercriticalcarbon dioxide with/without menthol: data correlation. *J. Supercrit Fluids.* **149**, 79–87. https://doi.org/10.1016/j.supflu.2019.03.020 (2019).

Acknowledgements

Acknowledgments: The authors extend their appreciation to Northern Border University, Saudi Arabia, for supporting this work through project number (NBU-CRP-2025-1497).

Author contributions

Conceptualization, S.A.S. and L.A.E.; methodology, A.N., and M.A.; software, A.N., and M.A.; validation, A.B., M.A., and L.A.E.; formal analysis, S.A.S., and M.A.; investigation S.A.S., L.A.E., A.N., and M.A.; resources, S.A.S.; data curation, S.A.S.; writ-ing—original draft preparation, A.N., and M.A; writing—review and editing, S.A.S. and L.A.E.; visualization, L.A.E., A.N., and M.A; supervision, S.A.S. and L.A.E.; project administration, S.A.S. and L.A.E.; funding acquisition, S.A.S. and M.A. All authors have read and agreed to the published version of the manuscript.

Declarations

Competing interests

The authors declare no competing interests.

Abbreviations.

AARD	Average absolute relative deviation
BCS	Biopharmaceutics Classification System
CEF	Cosolvent enhancement factor (CEF)
cEoS	Cubic Equations of State
DMSO	Dimethyl sulfoxide
GAS	Supercritical gas antisolvent
HBA	Hydrogen bond acceptor
HBD	Hydrogen-bond donor
PGSS	Particles from the gas saturated solution
MS·T	Méndez-Santiago and Teja
NHM	Nilotinib monohydrochloride monohydrate
RESS	Rapid expansion of supercritical solution
SAS	Supercritical antisolvent
SCF	Supercritical fluid
$scCO_2$	Supercritical carbon dioxide

.

Additional information

Supplementary Information The online version contains supplementary material available at https://doi.org/10.1038/s41598-025-20081-y.

Correspondence and requests for materials should be addressed to S.A.S. or L.A.E.